Research Paper

Combined film and impingement cooling of flat plate with reverse cooling hole

Kuldeep Singh [a], Udayraj [b], *

[a] Gas Turbine and Transmissions Research Centre, Nottingham University, Nottingham NG7 2TU, UK
[b] Department of Mechanical Engineering, Indian Institute of Technology Bhilai, Chhattisgarh 492015, India

A B S T R A C T

A numerical model is developed in the present work for analysing cooling performance of combined impingement-film cooling under realistic engine operating conditions. Effect of jet impingement along with the film cooling is analysed on fluid flow, heat transfer, cooling performance and pressure drop for forward and reverse orientations of the cooling hole. Further, effect of hole orientation on the cooling performance is studied under wide range of blowing ratios and jet-to-plate spacings. It is observed that the effect of jet impingement is significant on the cooling performance. Surface temperature of the metallic plate is found to be 50–90 °C lower for the combined jet impingement and film cooling case as compared to the only film cooling case. The improvement in the heat transfer for combined impingement-film cooling is at the cost of increased pressure drop. Film cooling effectiveness for the case of combined impingement-film cooling is found to be dependent on the hole orientation and blowing ratio. The secondary jet penetration into the mainstream increases with increase in the blowing ratio/velocity ratio. Kidney-vortices are formed at a velocity ratio of 1.07 from forward injection which resulted in decreased film cooling effectiveness. These kidney-vortices were not formed for the case of reverse injection and coolant spreads uniformly in the transverse direction. At lower velocity ratios when formation of kidney vortices is not prominent, forward injection results in better film cooling effectiveness compared to the reverse injection. Gas radiation is also considered in the modelling and its effect is found significant on the temperature prediction of the components.

Nomenclature

c_p	Specific heat (J/kgK)
D_f	Diameter of the film cooling hole (mm)
D_i	Diameter of the impingement hole (mm)
DR	Density ratio
e	Error, $e_a^{21} = \left\| \frac{vr_1 - vr_2}{vr_1} \right\|$
g	Grid
GCI	Grid convergence index, $\frac{1.25 e_a^{21}}{r_{21}^p - 1}$
h	Distance between jet and plate (mm)
htc	Heat transfer coefficient, $q''/(T_s - T_{c,in})$ (W/m²K)
I	Radiation intensity
L	Length of the cooling hole (mm)
M	Blowing ratio, $\frac{\rho_c}{\rho_{ms}} \frac{U_c}{U_{ms}}$
n	Refractive index
Nu	Nusselt number, $htc \times D_i / \lambda_{fluid}$
p	Apparent order of accuracy, $\frac{1}{\ln r_{21}} \left(\left\| \ln \left\| \frac{\epsilon_{32}}{\epsilon_{21}} \right\| \right\| + q(p) \right)$
q''	Wall heat flux (W/m²)
q(p)	$\ln \left(\frac{r_{21}^p - sa}{r_{32}^p - sa} \right)$
r_{21}	g_2/g_1
Re	Reynolds number based on mainstream flow and cooling hole diameter
t_c	Thickness of the thermal barrier coating (mm)
t_p	Thickness of the metallic plate (mm)
T	Absolute temperature (K)
T_{REC}	Recovery temperature, $T + (Pr)^{1/3} \frac{U^2}{2c_p}$ (K)
U	Horizontal velocity component (m/s)
V	Velocity magnitude (m/s)

Fig. 1. (a) Forward cooling hole and (b) reverse cooling hole arrangements.

VR	Velocity ratio, $\frac{U_c}{U_{ms}}$
vr	Critical variable (e.g. T, U)
x	Streamwise direction (m)
z	Spanwise direction (m)

Greek

α	Injection angle (degree)
β	Extinction coefficient
ε_{21}	vr2-vr1$\frac{T_{REC_{ms}}-T_S}{T_{REC_{ms}}-T_{REC_{sec}}}$
φ	Scattering phase function
η	Adiabatic effectiveness,
σ_s	Scattering coefficient$\frac{T_{ms}-T_{sec}}{T_{ms}-T_s}$
θ	Non-dimensional temperature,
ϕ	Overall effectiveness,$\frac{T_{REC_{ms}}-T_{TBC_S}}{T_{REC_{ms}}-T_{REC_{sec}}}$
ρ	Density (kg/m^3)
τ	Thermal barrier coating effectiveness,
μ	Dynamic viscosity (kg/ms)
λ	Thermal conductivity (W/mK)

Subscript

1, 2, 3	grid1, grid2, grid3
a	approximate
avg	area average
c	coolant
cl	centreline
f	film cooling
in	inlet
j	jet
ms	mainstream
s	surface
sec	secondary

Abbreviation

FH	Forward hole
RH	Reverse hole
FC	Film cooling
JI	Jet impingement

1. Introduction

Continuous push towards increasing the efficiency of turbo engines and higher thrust generation is essential to cope up with advancement of technology. Higher efficiency and thrust generation depend signifi-cantly on operating conditions and often lead to a high temperature and pressure working environment. Higher working temperature can se-verely impact life and performance of structural turbine components like turbine blades, turbine vanes, combustor liners, afterburner etc. Ef-fective protection for turbine components is required under such harsh working environments considering the material limitations. Reliable and safe operation of the gas turbine thus depends significantly on vari-ous cooling technologies and thermal barrier coating (TBC) which pro-tects structural components from harsh working environment and re-duces heat transfer to the components. Cooling technologies generally include impingement cooling, external film cooling or combined film-impingement cooling techniques. Jet impingement cooling is one of the effective cooling techniques used widely for thermal management in various applications including gas turbine engines [1,2]. Film cooling is another widely used and studied cooling technique for thermal protec-tion of hot section components of gas turbine [3]. In the film cooling, cold secondary fluid passes through cooling holes on the component surface and forms a relatively lower temperature fluid film between the surface and hot working environment so that the structural component can be protected. A more practical and widely used cooling technique is combined film-impingement cooling which incorporates both internal cooling through impingement and external cooling in the form of film cooling. Here, secondary fluid stream cools the internal surface of the structural component (turbine blade) first by the jet impingement cool-ing in the impingement chamber before going out through the film cooling holes to perform the external film cooling to protect surfaces from hot mainstream gases. It has been found that the combined film-impingement cooling is more effective compared to just film cooling [4-8]. This effect is more significant when the material is of high thermal conductivity [4] and in case of lower jet-to-plate spacing [7]. Large number of experimental and numerical studies have been done on com-bined film-impingement cooling of turbine blades [6,9-11], curved sur-faces [12-17] and flat plates [4,5,7,8,18-22].

Curvature of the plate surface can affect local flow field and cooling performance significantly. Li and Corder [12] analysed effect of plate surface curvature and its effect was found to be significant on local Nus-selt number in case of dual-jet in a row as compared to single-jet in a row case although no significant effect of curvature was noticed in overall heat transfer. As far as curved surfaces are concerned, studies have found only slight increment in the overall effectiveness by the ad-dition of impingement cooling in the combined film-impingement cool-ing [13]. The increased internal cooling due to impinging jet is dimin-ished by the reduced external cooling due to reduction in the coolant flow rate and increase in coolant temperature. Wei-hua et al. [14] stud-ied effect of blowing ratio, cooling hole orientation and jet-to-plate spacing on the cooling effectiveness and discharge coefficient for curved geometries. Better cooling effectiveness was observed at higher blowing ratio, lower hole angle and smaller jet-to-plate spacing. Effect of blowing ratio and film hole spanwise angle was analysed numerically by Liu et al. [15] for leading edge of a turbine blade. Blowing ratio found to affect the internal surface heat transfer coefficient and external
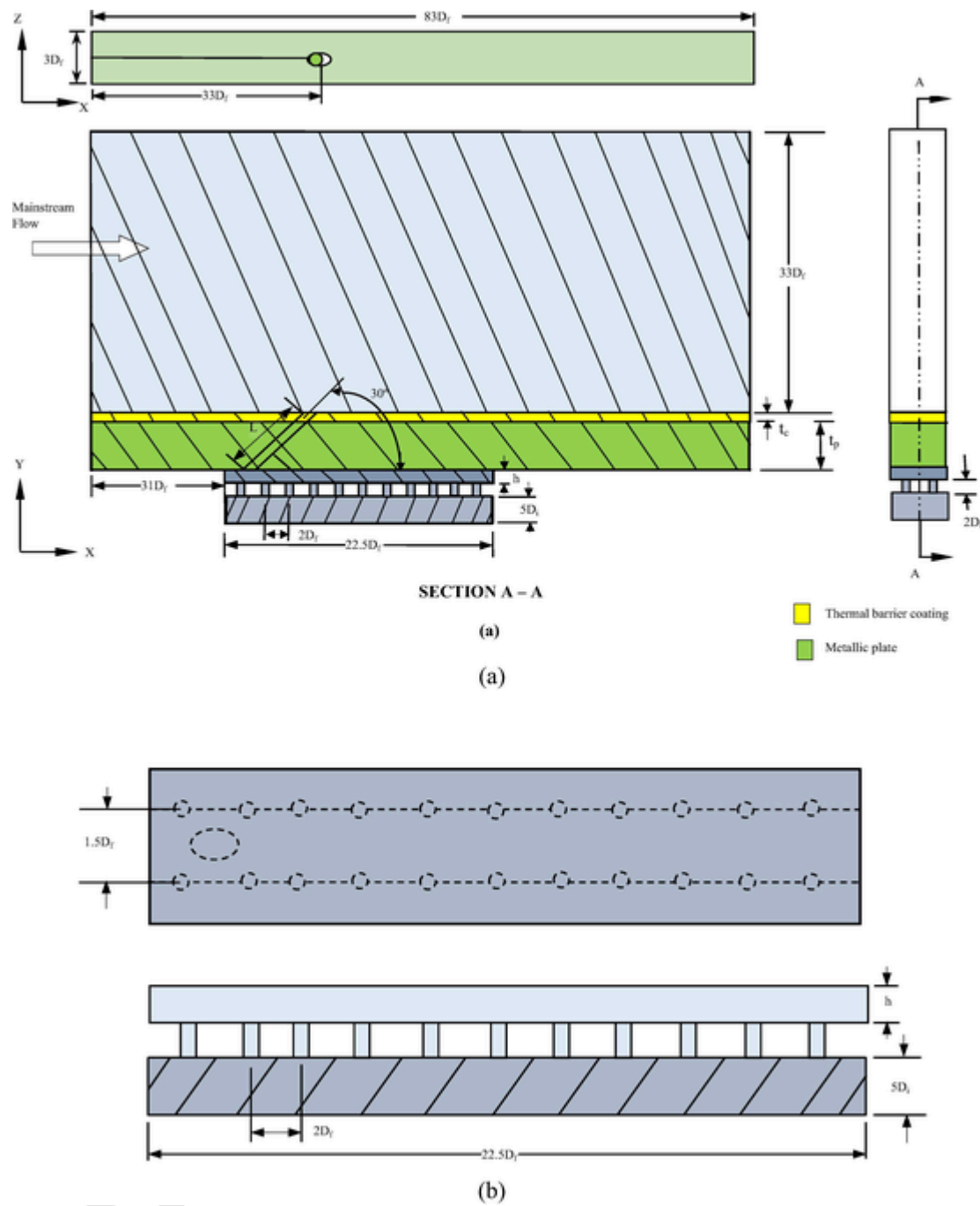
Fig. 2. (a) Film cooling hole arrangement on test plate and associated details (**figures not to scale**) (b) arrangement for coolant injection through impingement holes.

film cooling effectiveness significantly whereas effect of film hole spanwise angle was found to be more dominant on external film cooling effectiveness compared to internal surface heat transfer coefficient. Yang et al. [17] conducted experimental and numerical study to analyze cooling performance of an endwall experiencing conjugate heat transfer under realistic engine operating conditions. Effect of Reynolds number and mass flow rate was analyzed on the cooling performance.

As far as combined film-impingement cooling studies on flat plate are concerned, effect of geometric shape of cooling hole [18], orientation or inclination of cooling hole [19], blowing ratio [5,18,20-22], jet-to-plate spacing (h/D_i) [4,7,8,12,19-21], jet-spacing [12,20], Reynolds number [12], cooling hole arrangement [21], operating pressure [12], thermal barrier coating [10] and materials [4,5,7,8,20,22] was

analysed by various researchers in the past. Miao and Wu [18] numerically studied effect of three geometric shapes (cylindrical round simple angle, CYSA; forward-diffused simple angle, FDSA; and laterally diffused simple angle, LDSA) of cooling hole and blowing ratio (0.3 to 1.5) on the cooling performance. Significant effect of hole shape was observed on the adiabatic film cooling effectiveness and flow-field. The counter-rotating vortex pair (CRVP) was observed in CYSA and FDSA shaped holes whereas the same was not found in case of LDSA hole at higher blowing ratio. Effect of blowing ratio, h/D_i and cooling hole orientations (normal and forward inclined) was experimentally analysed by Oh et al. [19] considering conduction effect on the plate. The cooling effectiveness was found to be better in case of inclined cooling hole compared to normal cooling hole and effect of h/D_i was found to be

Table 1
Values and range of various parameters.

Parameter	Value
Metallic plate thickness, t_p (mm)	3.0
Thermal barrier coating thickness, t_c (mm)	0.5
Film cooling hole diameter, D_f (mm)	6.0
Film cooling hole length, L (mm)	6.0
Jet diameter, D_i (mm)	2.0
Ratio of jet-to-plate spacing and jet diameter, h/D_i	1.0 – 4.0
Reynolds number based on mainstream flow and cooling hole diameter, Re	22,750
Mainstream velocity (m/s)	100
Mainstream Pressure (bar)	15
Secondary air to mainstream pressure ratio	1.07
Blowing ratio, M	0.5 – 2.0
Mainstream temperature (K)	1375–1875
Density ratio, DR	2.75 – 3.75
Secondary air temperature (K)	500

more pronounced in case of inclined hole compared to normal cooling hole case. Jung et al. [8] also observed higher cooling effectiveness in case of inclined film cooling hole compared to the normal hole. Lee et al. [4] noticed that the effect of change in h/D_i was more pronounced on the downstream side in case of inclined cooling hole although there was not much variation in the overall cooling effectiveness. Jung et al. [21] also noticed that there was no effect of h/D_i on the cooling effectiveness. Cooling effectiveness is generally related to both blowing ratio and h/D_i. Mao et al. [20] noticed higher cooling effectiveness at higher h/D_i for lower blowing ratio (M = 0.0017–0.0023) and lower cooling effectiveness at higher h/D_i for higher blowing ratio (M = 0.0044–0.0066). Jung et al. [21] found that the cooling effectiveness decreases in the upstream region (due to the penetration effect of coolant) and it increases in the downstream region (due to accumulation of coolant and pushing effect) as blowing rate increases. Panda and Prasad [5] also observed significant rise in the cooling effectiveness in the upstream region with increase in blowing ratio whereas cooling effectiveness in the downstream region remained unaffected with the increase in the blowing ratio. Mensch et al. [10] found that introduction of thermal barrier coating (TBC) improves the cooling effectiveness of turbine blades more significantly than the increase in the blowing ratio and the improvement in the cooling effectiveness with the TBC increases with increase in the blowing ratio. Effect of cooling hole arrangement was also analysed in the few studies. It was found that the

staggered cooling hole arrangement results in better and uniform cooling compared to inline cooling hole arrangement [21].

Plate material also plays an important role in the effectiveness of combined film-impingement cooling. Lee et al. [4] compared effect of two plate materials (stainless steel and polycarbonate) on cooling effectiveness and higher cooling effectiveness was observed with stainless steel plate due to its higher heat conduction capacity. Cooling effectiveness with stainless steel and Perspex plate were also compared by Panda and Prasad [5]. They also noticed higher average cooling effectiveness in case of high conductivity (stainless steel) plate although the peak maximum local cooling effectiveness was found to be lower in case of stainless steel plate. Effect of three different plate materials (k = 0.2, 1.5, 15.0 W/mK) was analysed for various blowing ratio by Panda and Prasad [22] and it was found that the flow over the interacting surface influences cooling effectiveness more significantly for lower thermal conductivity plate material cases compared to higher thermal conductivity material case. It was also noticed that the temperature fluctuation and associated stresses can be reduced further by employing plate of higher thermal conductivity materials. High thermal conductivity plate material results in more uniform lateral cooling [7]. Jung et al. [7,8] further noticed that cooling effectiveness decreases with reduction in the plate thermal conductivity (or increase in the Biot number) due to decrease in the conduction contribution. Effect of blowing ratio on the cooling effectiveness is also affected by the plate material [16].

In the present study attention is focussed on combined film-impingement cooling where heat transfer on the inner and outer surface are accounted simultaneously along with conjugate heat transfer. A numerical model is developed to analyse cooling effectiveness. It is very clear from the literature that flow separation due to occurrence of counter-rotating vortices pair (CRVP) in forward oriented hole led to lower cooling effectiveness in case of film and combined film-impingement cooling [23]. Recently, effect of dimple on plate surface was analysed on flow field and cooling effectiveness and it was found that introducing dimple on the surface may lead to slight reduction in the CRVP and thus penetration of jet in the mainstream [23]. However, the effect of introducing dimple was found very minimal on CRVP strength reduction and negligible on the adiabatic film cooling effectiveness. Reverse cooling hole has been recently introduced to mitigate this effect in case of the film cooling [24,25]. Tong et al. [26] analysed effect of forward and reverse orientation of the cooling holes in case of combined film-impingement cooling of a flat metallic plate. It was observed that the reverse orientation of the cooling hole can lead up to 100 K decrease in the plate temperature and 31.79 % increase in the cooling effectiveness. Cooling performance is also affected by TBC, jet-to-plate spacing (h/D_i), density ratio and blowing ratio. It is not clear how cooling performance and plate temperature are affected with these
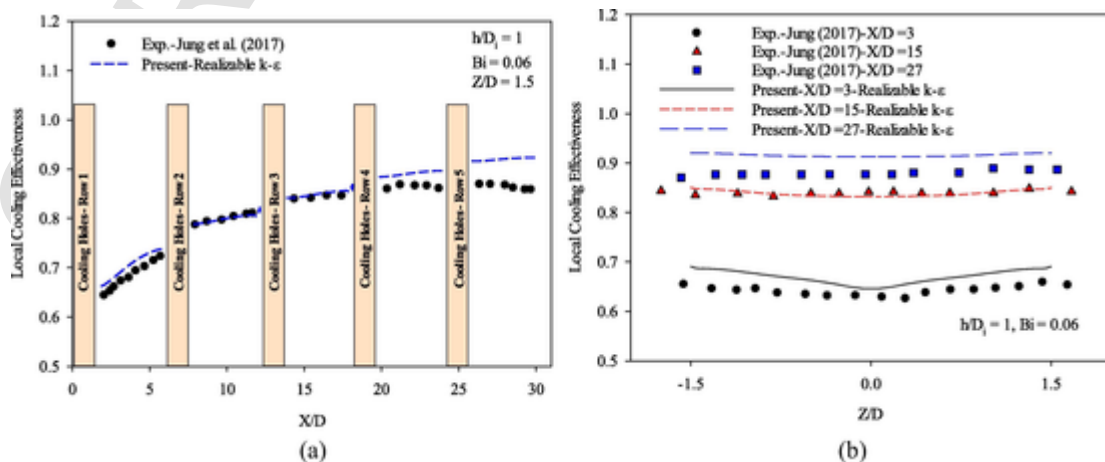
Fig. 3. Comparison of numerically obtained local cooling effectiveness in the (a) flow (longitudinal) and (b) lateral directions with the experimental measurements [8].
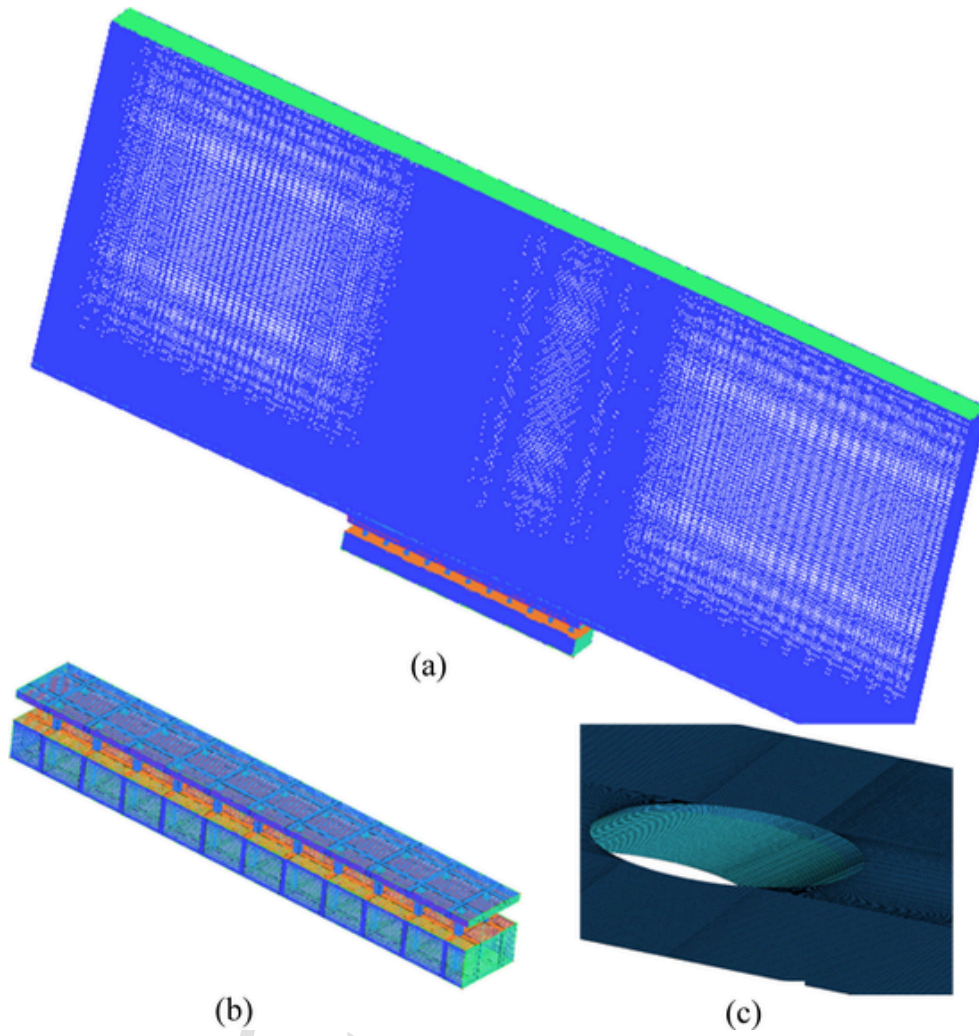
Fig. 4. Typical mesh in the (a) computational domain (b) impingement chamber (c) close to the film cooling hole.

parameters in case of reverse cooling hole orientation in combined film-impingement cooling applications. So, suitability of the reverse cooling hole for combined film-impingement cooling is investigated in the present work for the first time under various conditions considering realistic engine operating environment. Performance of the reverse and forward orientation of the film cooling hole is compared for various jet-to-plate spacing (h/D_i) and velocity/blowing ratios. Heat conduction in the plate and TBC is taken into consideration and effect of gas radiation is considered in the modelling.

2. Problem description

In this study, performance of reverse cooling hole configurations is analysed and compared with the forward cooling hole configuration for combined impingement and film cooling of a flat plate. These two cooling hole configurations are depicted in Fig. 1. One of the velocity components of the coolant is in the opposite direction to the mainstream flow for reverse cooling hole case. The computational domain includes film cooling hole of diameter D_f ($= 6$ mm) and a channel of height $33D_f$, through which mainstream air flows as shown in Fig. 2 (a). An inclined film cooling hole (30° with reference to mainstream air flow) is made through IN738 metallic plate of thickness t_p. Length of the film cooling hole is kept same as that of its diameter (i.e., $L/D_f = 1$). The metallic plate is coated with a 0.5 mm thick (t_c) Yettria stabilized zirconia (YSZ) thermal barrier coating towards the exposed side. Jet diameter (D_i) is taken as 2 mm. Ratio h/D_i is varied from 1.0 to 4.0. Secondary air enters

the impingement holes through a plenum as shown in Fig. 2 (b). Impingement holes are arranged in-line in 11 rows to cool the metallic plate internally. These impingement holes are aligned in staggered arrangement with respect to the cooling hole. Lateral pitch of the impingement hole is $1.5D_f$ and longitudinal pitch of the impingement holes is $2D_f$.

In this study, effect of jet impingement on film cooling, jet-to-plate spacing, and jet diameter ratio (h/D_i) and velocity/blowing ratio are analysed on cooling performance for forward and reversed cooling hole configurations. Values and range of various parameters considered in the present work are shown in Table 1. Further, effect of gas radiation is also studied on plate cooling effectiveness under realistic operating conditions of a gas turbine.

3. Numerical modeling

A three-dimensional numerical model is developed to analyse fluid flow and heat transfer associated with the combined film and impingement cooling of flat plate. Time-averaged equations considering steady, incompressible and turbulent flow are as follow:

$$\frac{\partial \left(\rho u_i \right)}{\partial x_i} = 0 \tag{1}$$

$$\frac{\partial \left(\rho u_j u_i \right)}{\partial x_j} = -\frac{\partial P}{\partial x_j} + \frac{\partial}{\partial x_j} \left[\mu \left(\frac{\partial u_i}{\partial x_j} + \frac{\partial u_j}{\partial x_i} \right) - \overline{\rho u_i' u_j'} \right] \tag{2}$$
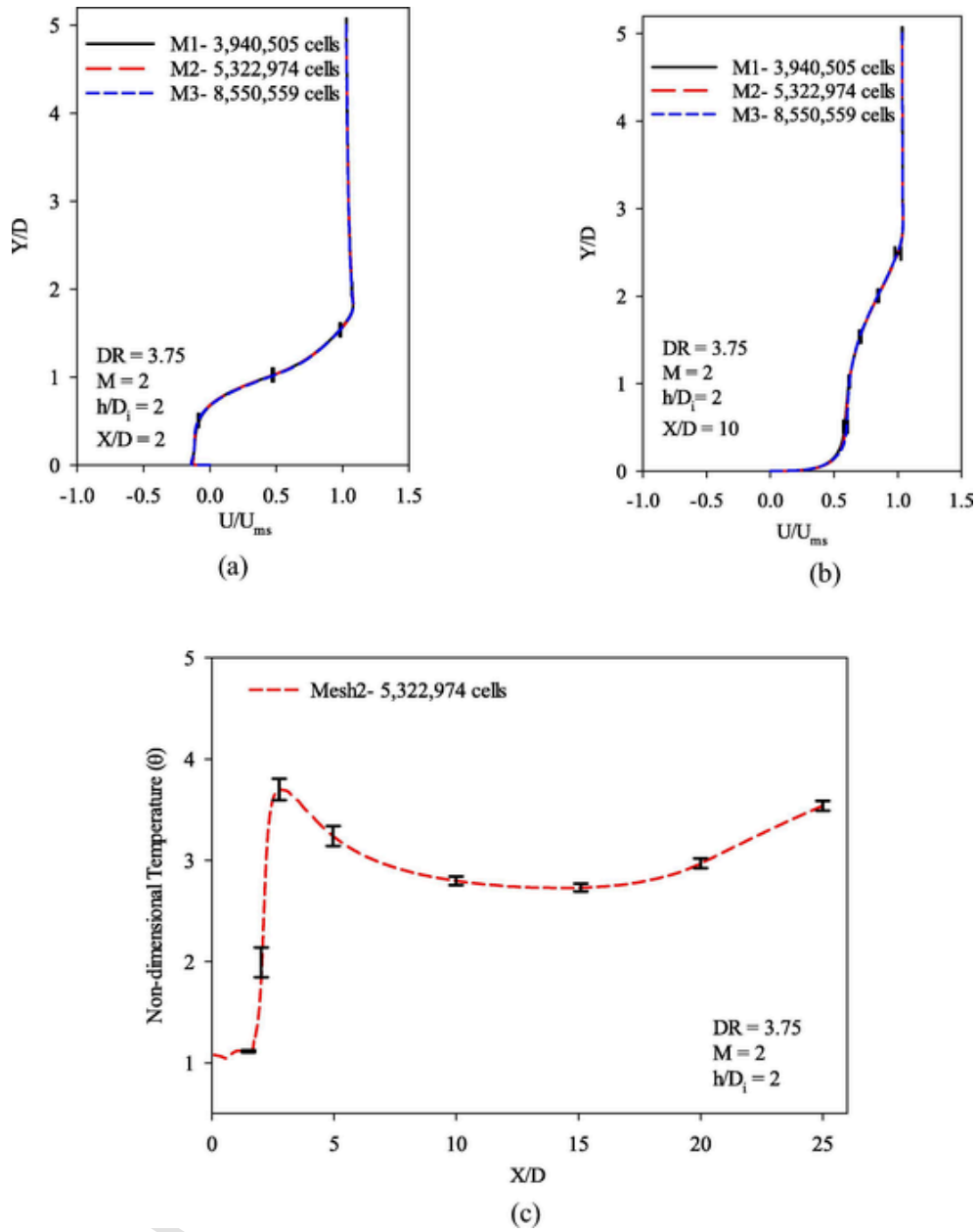
Fig. 5. Grid dependence study in case of forward injection configuration ($\alpha = 30°$) with $M = 2$, $DR = 3.75$ and $h/D_i = 2$.

$$\frac{\partial \left(\rho u_j T \right)}{\partial x_j} = \frac{\partial}{\partial x_j} \left[\frac{\mu}{\text{Pr}} \left(\frac{\partial T}{\partial x_j} \right) - \rho \overline{T' u_j'} \right] - \nabla.q_R \tag{3}$$

where, u, P and T are mean velocity, pressure and temperature, respectively. u' and T' are the fluctuating components of velocity and temperature, respectively. $-\rho \overline{u_i' u_j'}$ and $c_p \overline{T' u_j'}$ are the Reynolds stress tensor and specific turbulent heat fluxes which are calculated based on the Boussinesq hypothesis and the simple eddy diffusivity model as:

$$-\rho \overline{u_i' u_j'} = \mu_t \left(\frac{\partial u_i}{\partial x_j} + \frac{\partial u_j}{\partial x_i} \right) - \frac{2}{3} \rho k \delta_{ij} \tag{4}$$

$$\rho \overline{T' u_j'} = -\frac{\mu_t}{\text{Pr}_t} \frac{\partial T}{\partial x_j} \tag{5}$$

where, k, μ_t and Pr_t are turbulent kinetic energy, turbulent viscosity and turbulent Prandtl number, respectively. Previous studies have used low Reynolds number k-ε model [18], standard k-ε turbulence model

with enhanced wall function [12], and k-ω SST turbulence model [5,22] for combined film-impingement cooling of a flat plate. However, there are some studies [27] which suggest that the realizable k-ε turbulence model works well for such kind of problems. So, the realizable k-ε turbulence model is considered. The turbulent model is not discussed in detail here considering brevity. Readers are encouraged to refer Ref. [28] for more details of the turbulent model. $\nabla \cdot q_R$ is the divergence of the radiative heat flux which is obtained as [29]:

$$\nabla \cdot q_R = \kappa \left(4\pi I_b - G \right) \tag{6}$$

where, κ and I_b ($= \sigma T^4 / \pi$) are absorption coefficient and blackbody intensity, respectively. Irradiation (G) is defined as

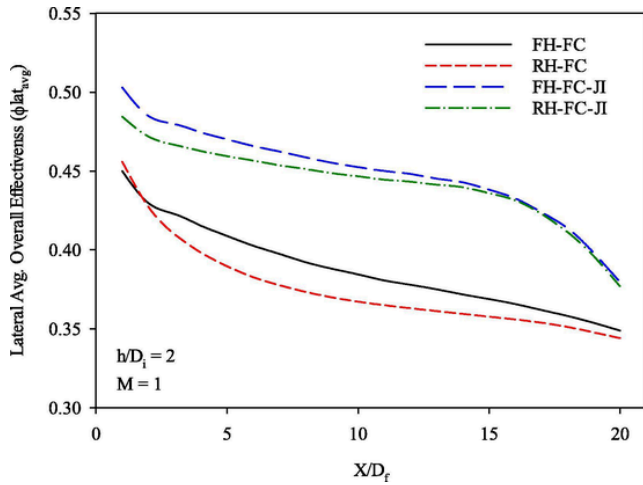$$G = \int_{\Omega=0}^{4\pi} I \left(\Omega \right) d\Omega \tag{7}$$

Fig. 6. Variation of the overall film cooling effectiveness along the longitudinal direction for the forward/reverse orientations of the cooling hole considering with and without jet impingement cases at $h/D_i = 2$ and $M = 1$ (or $VR = 0.267$).

where, Ω is the solid angle and I is the radiation intensity. Radiation intensity is obtained by solving the Radiative Transfer Equation (RTE), Eq. (8) using the discrete ordinates (DO) method.

$$(\vec{s} \cdot \nabla) I (\vec{r}, \vec{s}) = -\beta I (\vec{r}, \vec{s}) + \kappa n^2 I_b (T (\vec{r})) + \frac{\sigma_s}{4\pi} \int_{4\pi} I (\vec{r}, \vec{s'}) \varphi (\vec{s}, \vec{s'}) d\Omega' \tag{8}$$

Weighted-sum-of-gray-gases model (WSGGM) is used to compute radiative properties (absorption/emission coefficient) of the medium in terms of weighing factors and absorption coefficient of species. Details related to the implementation of DO method and WSGGM can be found in Ref. [28].

3.1. Material properties

In the present study, working fluid (mainstream and secondary fluid) is air and its density is calculated based on the ideal gas law as it is assumed to be an ideal gas. As fluid temperature varies considerably during the plate cooling process, fluid properties like thermal conductivity (λ), specific heat (c_p) and viscosity (μ) are considered to be temperature dependent [30]:

$$\lambda = \left(7.9957 \times 10^{-12}\right) T^3 - \left(2.4013 \times 10^{-08}\right) T^2 + \left(8.3047 \times 10^{-05}\right) T + \left(2.8822 \times 10^{-03}\right) \tag{9}$$

$$c_p = \left(9.0813 \times 10^{-11}\right) T^4 - \left(4.8066 \times 10^{-07}\right) T^3 + \left(8.0735 \times 10^{-04}\right) T^2 - 0.32136T + 1045 \tag{10}$$

$$\mu = \left(1.7020 \times 10^{-14}\right) T^3 - \left(4.0405 \times 10^{-11}\right) T^2 + \left(6.8539 \times 10^{-08}\right) T + \left(1.0616 \times 10^{-06}\right) \tag{11}$$

Properties of plate material (Nickel based alloy, IN738LC) are temperature dependent as plate temperature also varies significantly due to heat transfer from hot mainstream gases to the plate. Thermal conductivity and specific heat of the plate material in the temperature range 298–1773 K are taken as [31]:

$$\lambda = \left(2.31 \times 10^{-17}\right) T^6 - \left(1.33 \times 10^{-13}\right) T^5 + \left(3.12 \times 10^{-10}\right) T^4 - \left(3.78 \times 10^{-7}\right) T^3 + \left(2.52 \times 10^{-4}\right) T^2 - 0.0771T + 18.826 \tag{12}$$

$$c_p = -\left(5.8 \times 10^{-10}\right) T^4 + \left(2.06 \times 10^{-6}\right) T^3 - \left(2.53 \times 10^{-3}\right) T^2 + 1.197T + 234.2 \tag{13}$$

where, T in Eqs. (9)–(13) is temperature in Kelvin (K).

Thermal conductivity of the TBC considered in the present study is 2 W/mK following [27,32,33]. In order to simulate the effect of gas radiation, gas composition on mass basis of CO_2, H_2O, O_2 is taken as 12.38%, 4.96%, and 8.97%, respectively [27] for a fuel/air ratio of 0.0409 which represents rich fuel condition in aeroengine [34].

3.2. Boundary conditions

Velocity at the mainstream and secondary fluid inlets are specified based on the Reynolds number (Re) and blowing ratio (M), depending upon the case. Inlet temperatures are specified based on the density ratio (DR). Turbulence intensity of 5 % is specified at both the inlets considering actual engine conditions [35]. Zero pressure-gauge is taken at the outlet boundary which is assigned as pressure outlet. Periodic boundary conditions are assigned at the lateral boundaries of the computational domain. No slip wall boundary conditions are imposed at all the walls of the main and secondary ducts. Coupled boundary conditions are considered at thermal barrier coating wall and metallic plate to solve conjugate heat transfer. Continuity of temperature and heat flux are ensured at all the interfaces. For radiative heat transfer, emissivity at inlet and outlet of the duct is set to 0.5. The emissivity of the TBC and outer walls are taken as 0.8 and 1.0, respectively based on Wenping et al. [36] and Singh et al. [27].
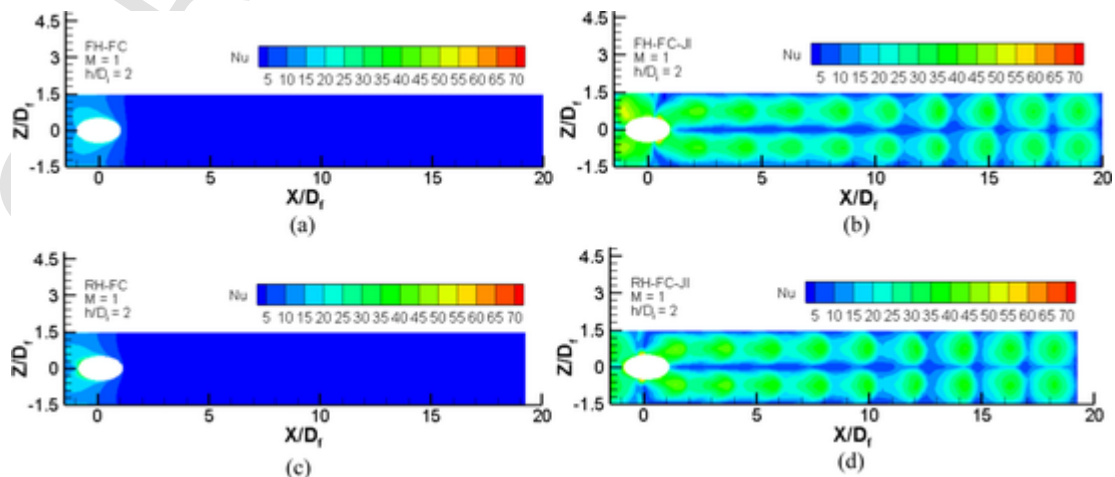

Fig. 7. Nusselt number contours at the bottom surface of the metallic plate for the forward and reverse cooling hole configurations with and without jet impingement.
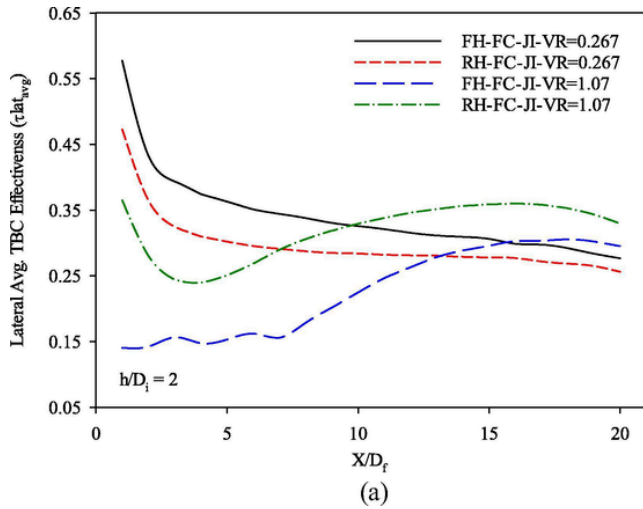
Fig. 8a. Variation of the lateral average TBC effectiveness along the longitudinal direction at $VR = 0.267$ ($M = 1$) and $VR = 1.07$ ($M = 4$) for $h/D_i = 2$, $DR = 3.75$.
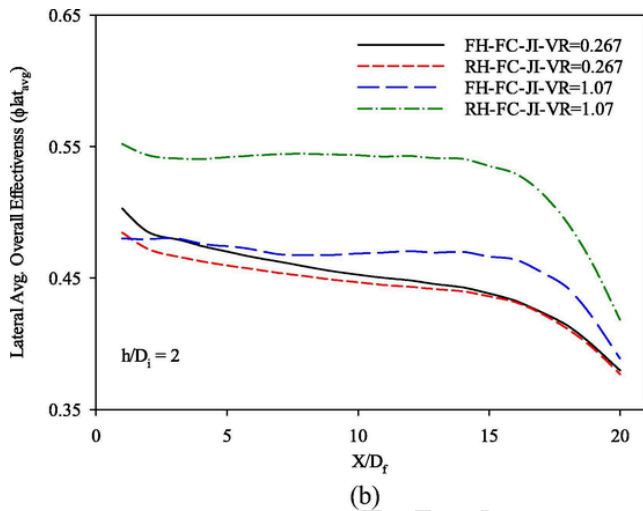

Fig 8b. Variation of the lateral average overall effectiveness along the longitudinal direction at $VR = 0.267$ ($M = 1$) and $VR = 1.07$ ($M = 4$) for $h/D_i = 2$, $DR = 3.75$.

3.3. Solution procedure

The governing equations, Eqs. (1)–(3), together with turbulence equations and RTE are solved using the finite volume method (FVM) based commercial CFD solver FLUENT. Thermo-physical properties of air and plate material are considered to be temperature dependent, Eqs. (9)–(13). All the governing equations are discretized using a second-order upwind interpolation scheme. Pressure-velocity coupling is ensured with the help of SIMPLE algorithm [37]. The solutions are considered to be converged if the residual becomes lower than 10^{-08} for energy equation and 10^{-05} for all the remaining equations.

3.4. Validation

Validation study is performed first to check reliability of the numerical modelling and to find out the appropriate turbulence model for the problem in hand. For this, all the geometric parameters and operating conditions were considered as per the experimental study of Jung et al. [8]. Experimentally and numerically obtained local cooling effectiveness in the longitudinal and lateral directions are shown in Fig. 3 (a)

and Fig. 3 (b), respectively. Fig. 3 (a) shows the comparison of the longitudinal variation of cooling effectiveness from experimental measurements [8] and present numerical results. Fig. 3 (b) shows the comparison of the lateral variation of cooling effectiveness obtained using the experimental measurements [8] and present numerical at different X/D values. It can be observed from the figures that the present numerical results agree well with the experimental observations for starting three rows of cooling holes. Thereafter, numerical results over-predicted film cooling effectiveness to a maximum value of 0.07 which corresponds to a temperature difference of 1.6 °C. The possible reason of this deviation is heat conduction from the plenum wall in the experimental study. In the numerical study, plenum walls were treated as adiabatic walls whereas in the experimental studies despite of insulation some heat is always conducted. Silieti et al. [38] also reported a better prediction of adiabatic and conjugate film cooling with the realizable k-ε turbulence model.

4. Results and discussion

Numerical study is conducted in the present study to analyse effect of cooling hole orientations (forward and reverse), blowing ratio and h/D_i on flow field and heat transfer in case of combined film and impingement cooling under realistic engine operating conditions. Effect of hole orientation is also analysed on cooling effectiveness and pressure drop for only film cooling, and combined film and impingement cooling cases. Effect of consideration of gas radiation is also studied.

4.1. Grid dependence study

Non-uniform structured grids generated using ICEM-CFD is considered. Finer grid is considered near the target walls to ensure y^+ values are less than or close to unity. Grid considered in this study for the entire computational domain, impingement chamber and near the film cooling hole is shown in Fig. 4 (a)-(c), respectively. Three grids with 3,940,505 cells (mesh1, M1), 5,322,974 cells (mesh2, M2) and 8,550,559 cells (mesh3, M3) are investigated for grid dependence study. Temperature distribution on the cooling plate and horizontal velocity close to the cooling hole are critical parameters in the present study. Hence, due care is given while refining grids in this area. It is ensured that grid refinement factor (r) in the critical zone is 1.5 following the recommendation of Celik and Li [39]. Grid dependence study is conducted for the forward orientation of the cooling hole with $M = 2$, $DR = 3.75$ and $h/D_i = 2$. Non-dimensional horizontal velocity (U/U_{ms}) and temperature (θ) are plotted in Fig. 5 at downstream distance of $X/D_j = 2$ and $X/D_j = 10$ along the centreline of the cooling hole i.e. $Z/D_j = 0.5$ for the forward injection configuration. Fig. 5 (a-b) show that the velocity distribution is identical for all the grids investigated. A maximum deviation of 2.54% in the non-dimensional velocity is observed at $Y/D_j = 0.5$, $X/D_j = 2$ between M1 and M2. At the same location, maximum difference in non-dimensional velocity between M2 and M3 is just 0.5%. Moreover, the maximum deviation in non-dimensional temperature between M1 and M2 is 26% at $Y/D_j = 0.5$, $X/D_j = 2$ and 0.67% between M2 and M3. These results suggest that the effect of refining grid beyond M2 is not significant and hence, M2 is selected for further study. Discretisation errors are quantified based on the grid convergence index (GCI) procedure proposed by Celik and Li [39]. The critical parameters i.e. non-dimensional velocity (U/U_{ms}) and non-dimensional temperature (θ) are selected for this analysis. The local order of accuracy (p) for non-dimensional velocity varies from $0.74 \leq p \leq 10.8$ at $X/D_j = 2$ and $0.258 \leq p \leq 5.05$ for $X/D_j = 10$ with the global average of 4.472 and 2.147, respectively. Likewise, local order of accuracy (p) for non-dimensional temperature is varied from 0.104 to 13.197 with the global average (p_{avg}) of 2.915. Numerical uncertainty due to discretisation errors is presented in terms of error bars in Fig. 5.
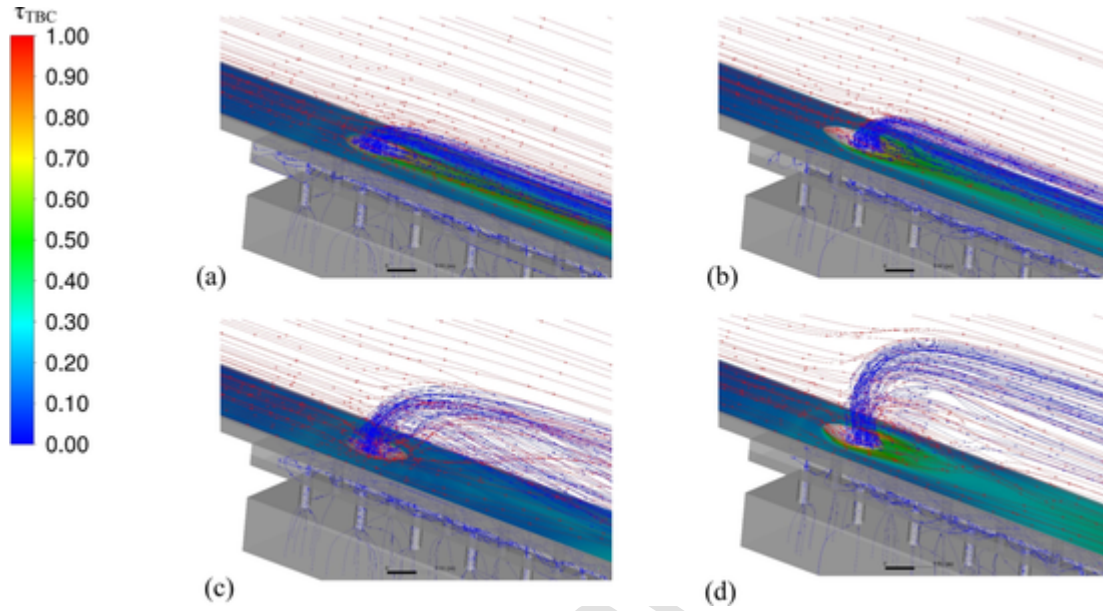
Fig. 9. Interaction of coolant jet with the mainstream near the cooling hole (a) Forward hole, $VR = 0.267$ (b) Reverse hole, $VR = 0.267$ (c) Forward hole, $VR = 1.07$ (d) Reverse hole, $VR = 1.07$.

4.2. Effect of jet impingement on cooling performance

Effect of jet impingement on film cooling effectiveness is discussed in this section. Fig. 6 shows the lateral average overall cooling effectiveness for the case involving just film cooling and film cooling with jet impingement where $h/D_i = 2$ and $M = 1$ ($VR = 0.267$). Results are presented in terms of lateral average film cooling effectiveness as it incorporates information of lateral spread of the cooling effect and provides realistic cooling performance. It is defined as:

$$\Phi_{lat,avg} = \int_{-1.5D_f}^{1.5D_f} \Phi_{lat} dz \qquad (14)$$

It can be observed that for both forward and reverse cooling hole configurations, cooling effectiveness increases because of the jet impingement. It means that the metallic plate can be maintained at a lower temperature with the introduction of the jet impingement. It is to be noted here that although the increase in lateral average overall effectiveness is approximately in the range 0.04–0.07, it corresponds to a significant cooling and decrease in the metallic plate temperature due to introduction of jet impingement with the film cooling. For example, increase of 0.04 and 0.07 in the overall cooling effectiveness corresponds to decrease of the metallic plate temperature by approximately 51 °C and 89 °C, respectively. Considering the fact that elevated temperature can significantly enhance chances of creep failure and degradation of the components by fatigue and hot corrosion [40,41], the impact of jet impingement on film cooling can be significant on the stability, reliability and life of the components due to significant drop in the metallic plate temperature. Cooling performance in case of the film cooling with jet impingement is higher compared to only the film cooling case because of increase in convective heat transfer from the bottom side of the metallic plate due to the jet impingement. This can be noticed from Fig. 7 which shows the comparison of the Nusselt number distribution for the film cooling (FC) and film cooling with jet impingement (FC-JI) cases for forward (FH) and reverse (RH) cooling hole configurations. It is evident that the Nusselt number of the bottom surface of the metallic plate increases significantly due to the jet impingement in the forward and reverse cooling hole configurations. It is to be noted that the cooling due to the jet impingement at the lower surface of the metallic plate is independent of the orientation of the film cooling hole.

Hence, overall film cooling effectiveness is found to be similar in both the cooling hole configurations. Considering the fact that the film cooling with jet impingement provides better cooling performance compared to only film cooling case, further analysis in subsequent sections is carried out in the present study considering the film cooling with jet impingement case.

4.3. Effect of forward and reverse orientations of the cooling hole on the cooling performance

Figs. 8a–b shows the variation of the lateral average TBC effectiveness and overall effectiveness in case of $h/D_i = 2$ and $DR = 3.75$ for the film cooling with jet impingement involving forward and reverse orientations of cooling hole. The results are shown at two different velocity ratios (VR) 0.267 and 1.07 which corresponds to the blowing ratios (M) of 1.0 and 4.0, respectively. At lower VR ($VR = 0.267$), both lateral average TBC effectiveness and lateral average overall effectiveness are lower in case of reverse orientation of the cooling hole compared to the forward orientation. This is primarily due to the fact that the secondary cooling fluid remains more attached to the metallic plate at lower VR in case of forward orientation of the cooling hole compared to the reverse cooling hole in which is clear from Fig. 9 (a)-(b) and temperature contours in Fig. 10 (a)-(b). It can also be noticed that the spread of coolant in the lateral direction is better in case of reverse cooling hole compared to the forward cooling hole. This results in slightly better cooling in the lateral directions in case of reverse cooling hole which is evident from the TBC cooling effectiveness contours shown in Fig. 11 (a)-(b). No significant effect of the two cooling hole orientations is noticed on the cooling performance of the bottom surface of the metallic plate as shown in the Nusselt number contours in Fig. 12 (a)-(b).

Contrary effect of the cooling hole orientations was noticed on the cooling effectiveness at higher value of the velocity ratio considered in the study ($VR = 1.07$). Lateral average TBC effectiveness and overall effectiveness is found to be significantly higher for the reverse orientation of the cooling hole compared to the forward orientation of the cooling hole as shown in Figs. 8a–b. Similar results were also obtained by Tong et al. [26] for effusion cooling case although the velocity ratio was not explicitly mentioned in their study. This is primarily due to the formation of the counter-rotating kidney vortex in case of the forward
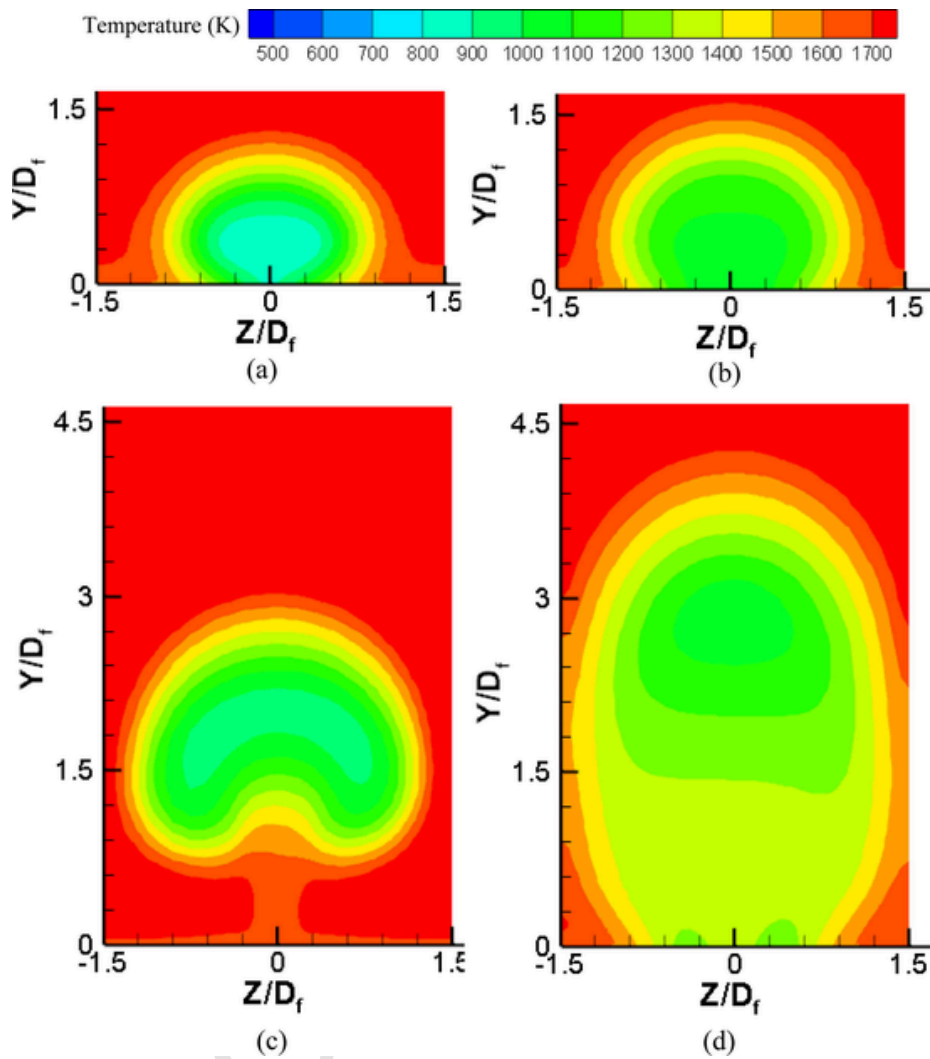
Fig. 10. Temperature contours at $X/D_f = 2$, depicting jet lift off (a) Forward hole, $VR = 0.267$ (b) Reverse hole, $VR = 0.267$ (c) Forward hole, $VR = 1.07$ (d) Reverse hole, $VR = 1.07$.
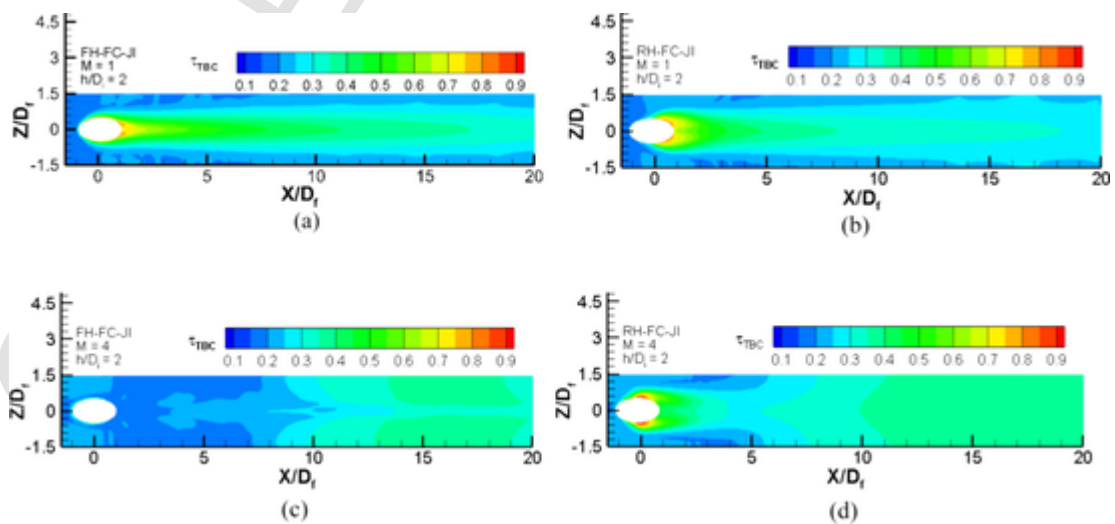

Fig. 11. TBC effectiveness contours for the (a) Forward hole, $VR = 0.267$ (b) Reverse hole, $VR = 0.267$, (c) Forward hole, $VR = 1.07$ (d) Reverse hole, $VR = 1.07$.
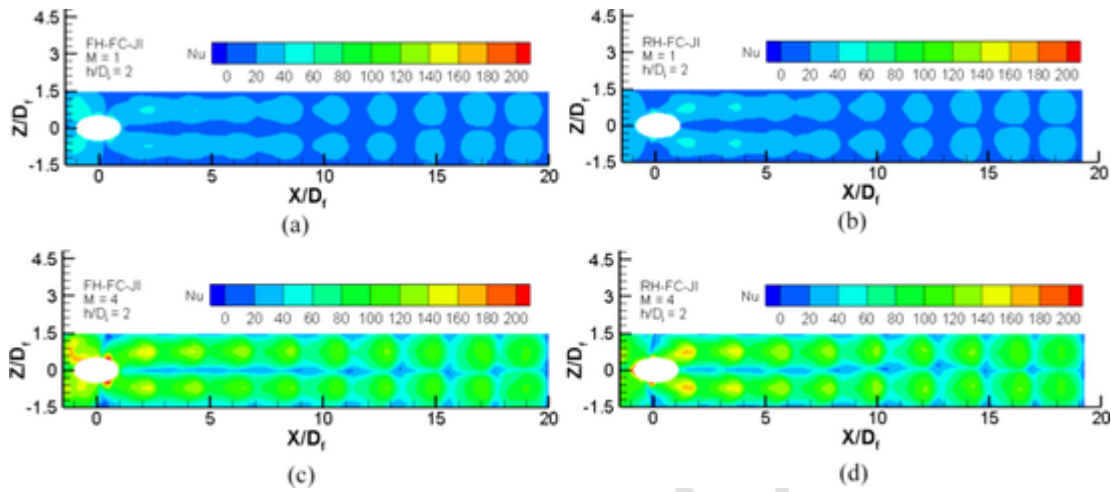
Fig. 12. Nusselt number contours on the bottom surface of the metallic plate for the forward and reverse cooling hole orientations at two different velocity ratios ($VR = 0.267$ and $VR = 1.07$).
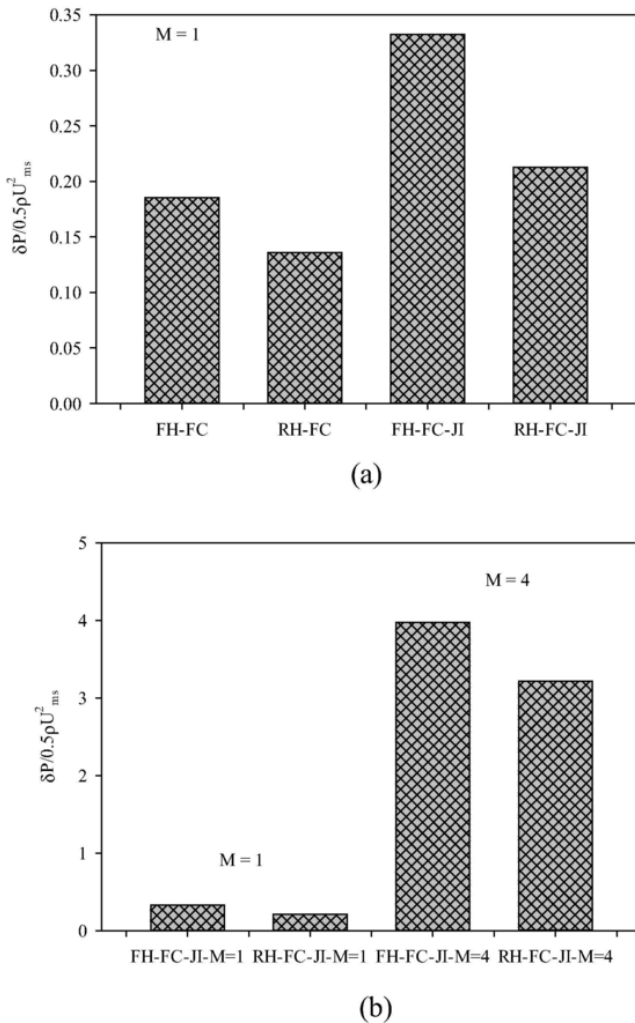

Fig. 13. Non-dimensional pressure drop for (a) $M = 1$ with and without jet impingement cooling, (b) $M = 1$ and $M = 4$ with jet impingement cooling.

cooling hole orientation at the higher secondary flow velocities. Fig. 9 (c) show that at higher VR the penetration of the secondary cooling fluid is significantly higher in case of the forward cooling hole. Due to this, the cooling fluid does not come in contact with the hot metallic surface for significant downstream distance along the flow direction in

case of the forward orientation of the cooling hole. Further, separation of the cooling fluid from the surface and its interaction with the mainstream flow leads to the formation of counter-rotating kidney vortex and negligible cooling of the hot surface near the cooling hole as shown in Fig. 10 (c) and Fig. 11 (c). Far away from the cooling hole, cooling fluid again comes in contact with the surface and cools the surface. So, the cooling effectiveness is lower near the cooling hole and it increases far away from the cooling hole along the longitudinal flow direction as evident from the contour of TBC cooling effectiveness in Fig. 11 (c). Similar trend was observed by Singh et al. [42] on the cooling effectiveness of a corrugated surface.

In case of the reverse orientation of the cooling hole at the higher VR ($VR = 1.07$), although the penetration of the cooling fluid is still higher, it is important to note that significant amount of the cooling fluid remain in contact with the hot surface throughout the plate downstream of the cooling hole as shown in Fig. 9 (d) and Fig. 10 (d). Further, due to the opposite flow direction of the cooling fluid compared to the mainstream fluid, the lateral spread of the cooling fluid is significantly higher in case of the reverse orientation of the cooling hole which can be noticed from the temperature contour shown in Fig. 10 (d). As the cooling fluid remains attached to the hot surface downstream the cooling hole, significantly better cooling can be observed throughout the plate in case of the reverse cooling hole which is evident from higher TBC cooling effectiveness in Fig. 11 (d). Moreover, better spread of the cooling fluid in case of the reverse cooling hole results in uniform cooling in the lateral direction throughout the plate.

Effect of the cooling hole orientation on cooling of the bottom surface of the metallic plate due to jet impingement is found insignificant as shown in Fig. 12. It can be seen that the Nusselt number distribution remains more or less similar for both the forward and reverse orientations of the cooling hole. However, effect of velocity ratio or blowing ratio is found to be very significant on the cooling of the bottom surface of the metallic plate. Nusselt number increases as the velocity ratio (or blowing ratio) increases in both the orientations due to increase in the impingement velocity at the bottom surface of the metallic plate. Increased cooling of the bottom surface of the metallic plate due to the jet impingement at the higher blowing ratio causes higher heat transfer and lower temperature of the top surface of the metallic plate due to conjugate heat transfer. It increases the overall cooling effectiveness of the metallic plate at higher velocity ratio as shown in Fig. 8b. Overall cooling effectiveness drops significantly at higher X/D_f due to the lower cooling of the exposed TBC surface by the cooling fluid due to increase in its temperature in the longitudinal direction as it absorbs heat from the exposed surface and mix with the mainstream fluid.
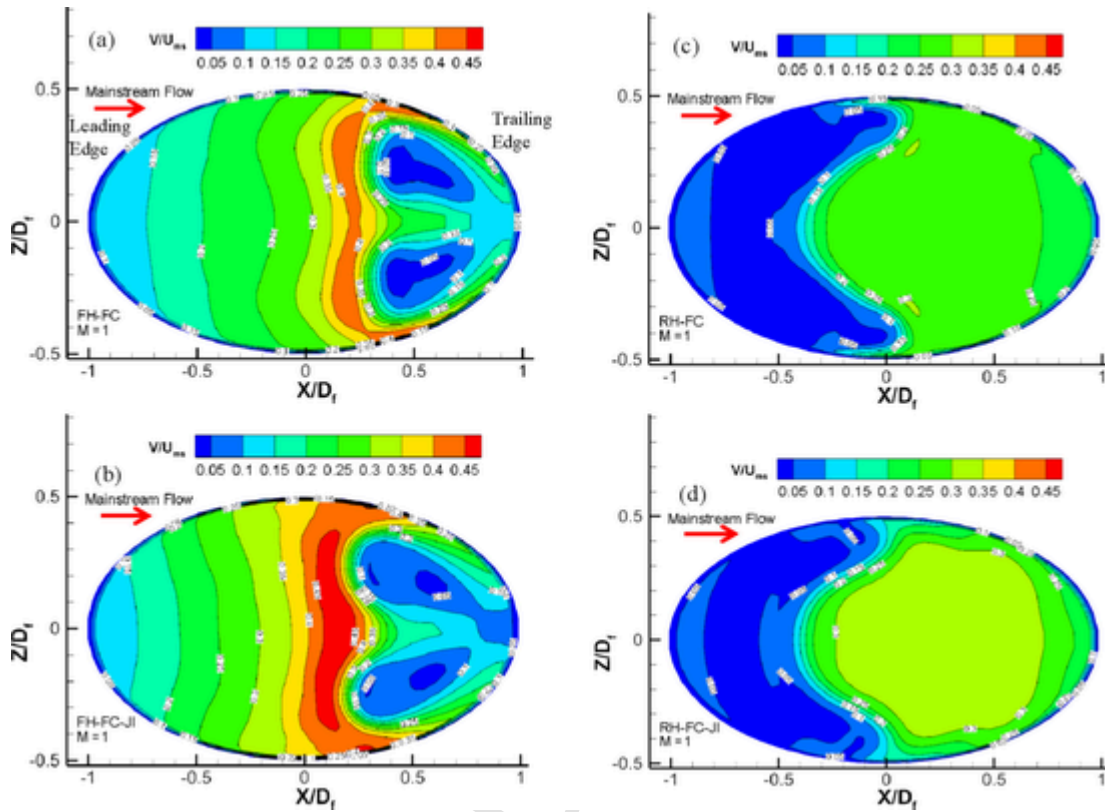
Fig. 14. Hole blockage for forward and reverse injection without jet impingement (a, c) and with jet impingement (b, d).

It can be seen from Fig. 8a that at lower velocity ratio ($VR = 0.267$), the TBC cooling effectiveness drops significantly just after the cooling hole in the longitudinal direction (till $X/D_f \approx 2.0$) in case of both forward and reverse cooling hole orientations. It is due to sudden increase in the cooling fluid temperature after absorbing heat from the hot metallic plate and mainstream hot fluid. Similar phenomenon can also be observed in case of reverse cooling hole orientation at the higher velocity ratio ($VR = 1.07$). In this case however, the cooling effectiveness increases later along the flow direction due to increased cooling of the bottom surface of the metallic plate due to higher impingement velocity and better attachment of the cooling fluid at the upper exposed TBC surface. Whereas the TBC effectiveness remains almost uniform in case of forward hole with higher velocity ratio ($VR = 1.07$) till a sufficient downstream distance (up to $X/D_f \approx 7$). It is primarily due to the two contradictory phenomena occurring in this case at the exposed TBC surface and bottom surface of the metallic plate with jet impingement. Here, heat transfer at the upper exposed TBC surface decreases due to the formation of the counter rotation kidney vortex formation and higher penetration of the cooling fluid at higher velocity ratio with the forward cooling hole orientation. On the other hand, due to higher impingement velocity at higher velocity ratio, Nusselt number and heat transfer rate from the bottom surface of the metallic plate increases. These rather contradictory heat transfer phenomenon at the exposed TBC surface and bottom surface of the metallic plate results in no significant change in the TBC effectiveness for a significant portion of the surface in case of forward cooling hole at the higher velocity ratio.

4.4. Effect of jet impingement and cooling hole orientations on the pressure drop

Pressure drop from the imping jet on a flat plate were investigated by Levy et al. [43] and Penumadu and Rao [44]. Levy et al. [43] proposed sum of local resistance approach to estimate the pressure drop because of the impinging jets. It was assumed that the total pressure

drop is sum of the pressure drop at the nozzle inlet, nozzle outlet, frictional losses in the nozzle and losses in the channel. However, in the case of combined jet impingement and film cooling; total pressure drop will be sum of pressure drop at the inlet and exit of the film cooling hole, frictional losses in the cooling hole and pressure drop because of the hole blockage.

Pressure drop of various cases is analysed here considering the pressure drop in the film cooling hole and in the impingement holes. For the sake of comparison, non-dimensional pressure drop is presented here which is obtained with respect to the mainstream flow parameters. Fig. 13 shows the non-dimensional pressure drop in case of the forward and reverse cooling hole orientations for film cooling with and without jet impingement at $M = 1$ and with combined jet impingement and film cooling at $M = 4$. It can be observed from Fig. 13 (a) that the pressure drop increases because of the jet impingement for both forward and reverse orientations. An increment of 79.27 % and 56.51% in the pressure drop is observed for the forward and reverse orientation because of the jet impingement at $M = 1$. This signify that the jet impingement section has a significant impact on the pressure drop or the pumping power required to inject coolant. Moreover, only a little difference (1% to 1.5%) in the pressure loss is observed when hole to impingement spacing is varied from $h/D_i = 1$ to $h/D_i = 4$. Hence, results are presented for $h/D_i = 2$ to avoid repetition of the results.

A comparison of non-dimensional pressure drops for the combined jet-impingement and film cooling configuration at $M = 1$ and 4 is presented in Fig. 13(b). The jet Reynolds number based on the impingement hole diameter and coolant fluid properties for these two blowing ratios are 8,800 and 35,200. The non-dimensional pressure increases by approximately 10 times as the blowing ratio is increased from $M = 1$ to $M = 4$. A parabolic increment in the pressure drop with the increase in the jet Reynolds number has been reported from the impinging holes, Penumadu and Rao [44]. Apart from that, the interaction of jet emerging from the cooling hole also changes with the increment of the blowing ratio. Jet penetration in the crossflow increases with the increase in
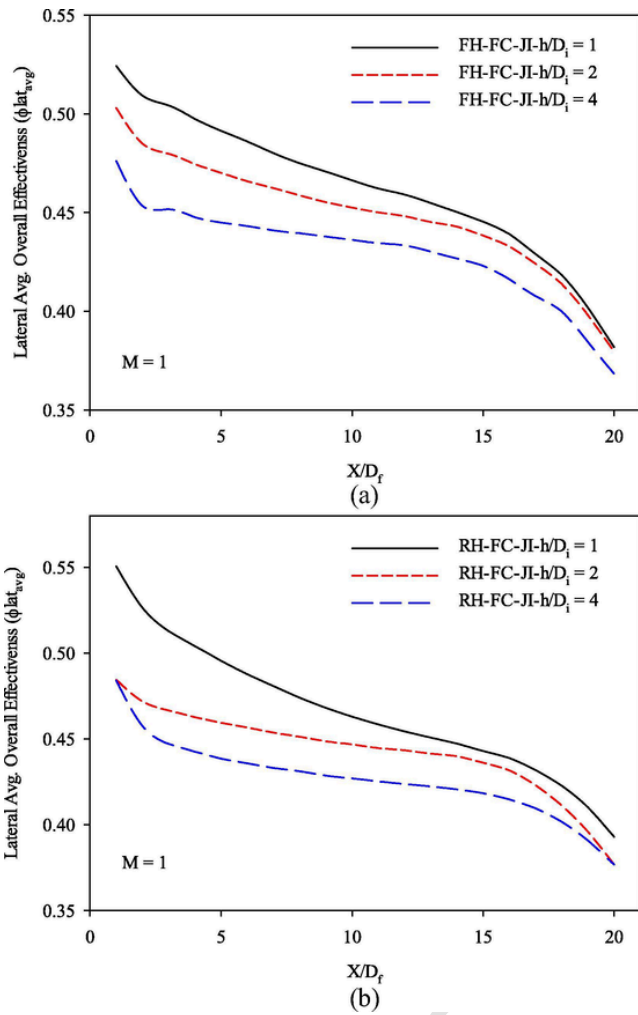
Fig. 15. Effect of h/D_i on the film cooling effectiveness for (a) forward orientation and (b) reverse orientation.

the blowing ratio. Both factors contributed to the significant increment of the pressure drop at a higher blowing ratio.

The blockage of the film cooling hole by the crossflow without and with the jet impingement for both forward and reverse orientation in case of only film cooling and combined impingement-film cooling are shown in Fig. 14. The comparison Fig. 14(a) with Fig. 14(b) and Fig. 14 (c) with Fig. 14(d) shows a similar qualitative trend for without and with jet impingement cases in both the hole orientations. However, it can also be observed that the maximum velocity increases because of the jet impingement for both the cooling hole orientations. In this study, the cooling hole is arranged in a staggered pattern from the jet impingement hole. Although, the impinging jet is not directly entering into the cooling hole, but it alters the flow pattern near the entrance region of the cooling hole. Consequently, velocity pattern changes in the case of jet impingement. This behaviour is prominent for the forward orientation as compared to the reverse orientation. In the case of forward orientation, coolant jet is splitted into two parts (low velocity region) in the cooling hole itself near the trailing edge. The extension of these low velocity regions is: $X/D_f = 0.4$ to 1 for the case without jet impingement. This low velocity region is further extended to $X/D_f = 0.2$ for the case with the jet impingement. A maximum velocity contour is observed upstream of this low velocity region for both the cases i.e. film cooling without and with jet impingement. However, the velocity contours of the reverse cooling hole orientation without and with jet impingement, Fig. 14 (c & d) shows that the hole is blocked towards the leading edge. The velocity gradient along the cross section of the holes is not as sharp as that for the forward holes. Consequently, the pressure drop in the reverse hole orientation is less as compared with the forward hole for the investigated range of blowing ratios at the operating conditions of gas turbine considered.

4.5. Effect of spacing from the jet exit to the plate (h/D_i)

For the jet impingement, the spacing from the jet exit to the plate (h) is one of the important parameters. In the literature, some study such as Lee et al. [4], Jung et al. [21] found insignificant effect of the variation in the h/D_i on the overall film cooling effectiveness whereas other studies such as Mao et al. [20] reported impact of h/D_i on the overall effectiveness. In the present study, it was decided to investigate the effect of h/D_i on the film cooling effectiveness for both the forward and reverse orientations by varying h/D_i in the range of 1 to 4. This range is selected
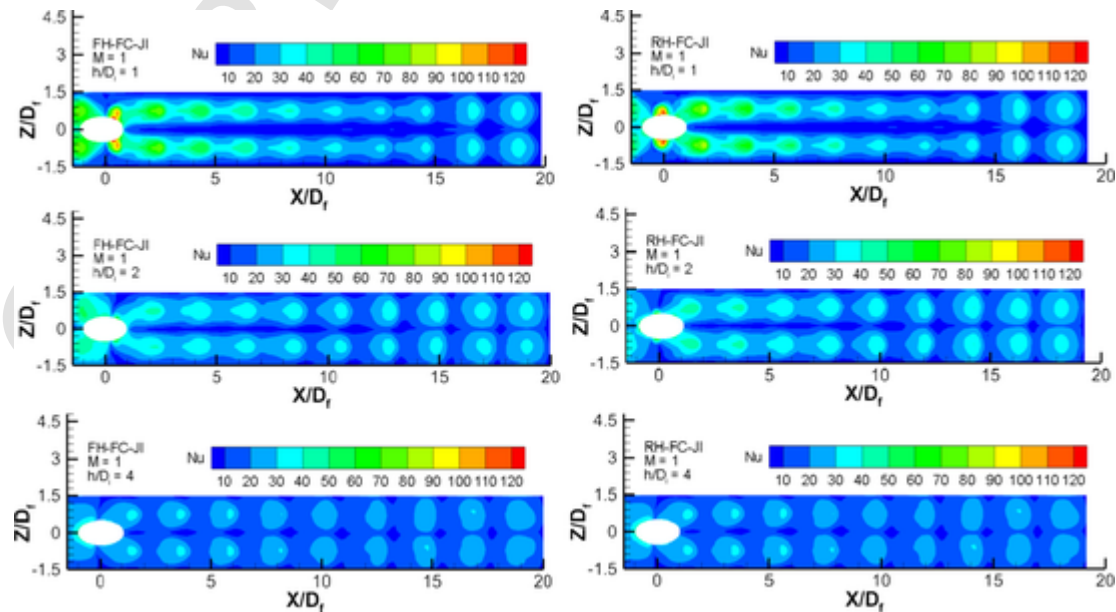

Fig. 16. Nusselt number contours on the bottom surface of the metallic plate for different h/D_i.
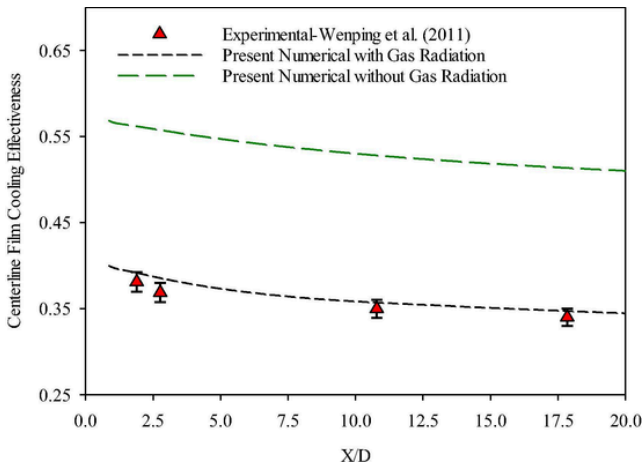
Fig. 17. Comparison of present numerical results with the experimental results of Wenping et al. [36] considering gas radiation and without gas radiation.
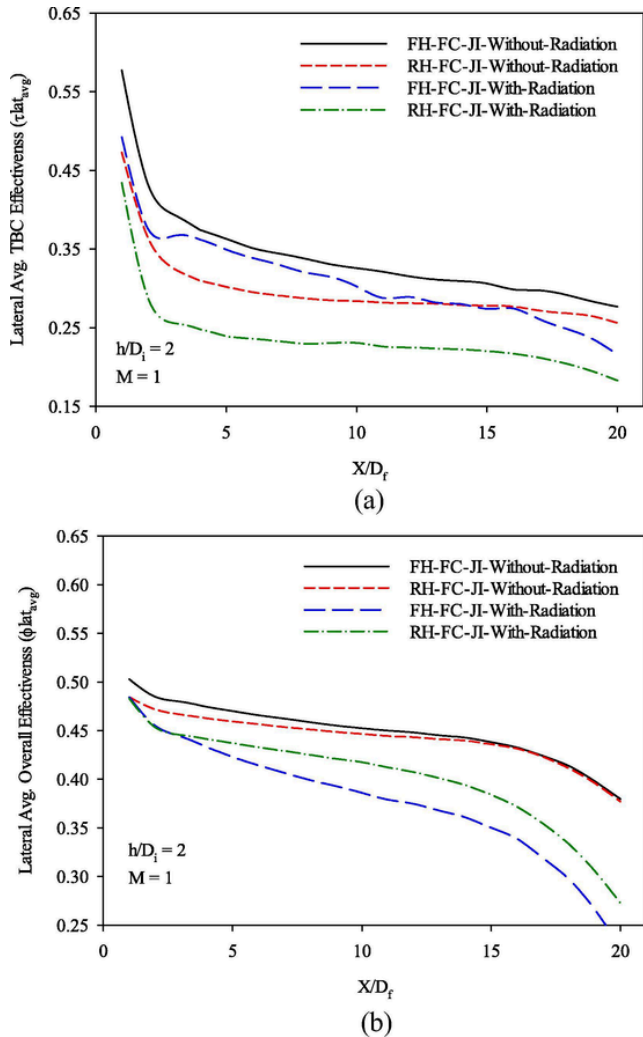

Fig. 18. Effect of gas radiation on the (a) TBC film cooling effectiveness (b) Overall film cooling effectiveness.

considering the space constraint in the case of gas turbine blades. The effect of h/D_i on the lateral average overall film cooling effectiveness is shown in Fig. 15. It can be observed that the lateral average overall film cooling effectiveness is higher at $h/D_i = 1$ as compared to the other investigated h/D_i for both the orientations. The improvement in the effec-

tiveness is higher towards the cooling hole and it decreases along the downstream direction. An improvement of 10%, 6.4% and 3.63% in the lateral average film cooling effectiveness is observed for $h/D_i = 1$ as compared to $h/D_i = 4$ at $X/D_f = 1$, 10 and 20 for the forward orientation. For the reverse orientation, the improvement is 13.73%, 8.46% and 4.27% in the lateral average film cooling effectiveness is observed for $h/D_i = 1$ as compared to $h/D_i = 4$ at $X/D_f = 1$, 10 and 20. The contours of Nusselt number for the investigated h/D_i ratios are shown in Fig. 16. A higher rate of heat transfer from the metallic plate is observed due to the impact of cooling jet at $h/D_i = 1$ this eventually results in the better film cooling effectiveness.

4.6. Effect of gas radiation

The effect of gas radiation on the film cooling effectiveness for the forward and reverse cooling hole is investigated at a blowing ratio of 1, $h/D_i = 2$ for engine representative conditions. Before analysing the effect of gas radiation on the combined jet impingement and film cooling configuration, numerical methodology considering gas radiation is validated against the benchmark test case of Wenping et al. [36]. Centreline film cooling effectiveness obtained from the present numerical model with and without gas radiation in plotted in Fig. 17 along with the experimental results of Wenping et al. [36]. It can be observed that film cooling effectiveness is in good agreement with the experimental results when effect of gas radiation is considered. Film cooling effectiveness is overpredicted when effect of gas radiation is ignored.

The lateral averaged TBC effectiveness and overall effectiveness is shown in Fig. 18 (a) and Fig. 18 (b), respectively for the investigated conditions. Both the TBC and overall effectiveness decreases when gas radiation effects are considered. A maximum drop of 22% in the TBC effectiveness is observed at $X/D_f = 20$ for the forward injection and 28% for the reverse injection because of the gas radiation.

This drop in TBC effectiveness is corresponding to a temperature rise of 77 K and 97 K respectively for forward and reverse injection at the TBC wall. On an average, a temperature rise of 50 K to 75 K is observed on the TBC wall when gas radiation effects were considered. A maximum drop of 40% in the overall effectiveness is observed at $X/D_f = 20$ for the forward injection and 28% for the reverse injection because of the gas radiation. This drop in overall effectiveness is corresponding to a temperature rise of 194 K and 134 K respectively for forward and reverse injection at the metallic plate. On an average, a temperature rise of 94 K to 54 K is observed on the metallic plate when gas radiation effects were considered. Singh et al. [27] and Ren et al. [45] also reported an increment in the surface temperature while considering gas radiation. The contours of TBC effectiveness for the forward and reverse injection case without considering and with consideration of the gas radiations effects confirm the reduction in TBC effectiveness as shown in Fig. 19.

5. Conclusions

In the current study, cooling effectiveness is analysed and compared considering only film cooling and combined impingement-film cooling. Effect of forward and reverse orientations of the cooling hole is analysed on the cooling performance and pressure drop under different blowing ratios. Effect of h/D_i and consideration of gas radiation is also discussed for the combined impingement-film cooling of a flat plate. Cooling effectiveness increases due to the jet impingement in case of combined impingement-film cooling in forward as well as reverse orientations of the cooling hole. This increment in the cooling effectiveness is at the expense of the pressure drop. An increment of 79.27 % and 56.51% in the pressure drop is observed for the forward and reverse orientation because of the jet impingement at $M = 1$.

Cooling performance is found to be better at lower h/D_i for both the forward and reverse orientations of the cooling hole. An improvement
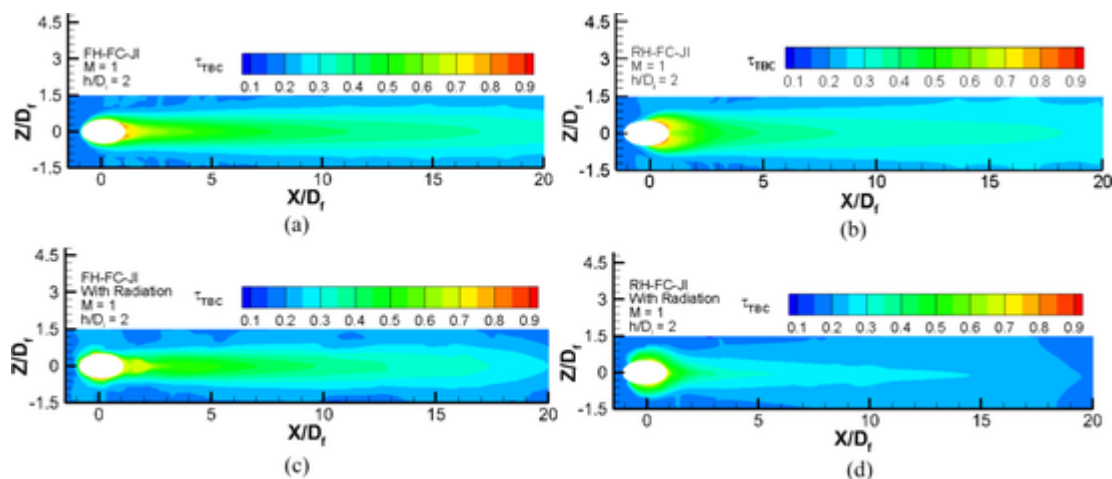
Fig. 19. TBC effectiveness contours for the forward and reverse cooling hole orientations with and without considering the effect of gas radiation.

of 10 % and 13.73 % in the lateral average film cooling effectiveness at $X/D_f = 1$ is observed for $h/D_i = 1$ as compared to $h/D_i = 4$ in case of the forward and reverse orientations, respectively. Gas radiation effect is significant on the overall cooling effectiveness. A maximum drop of 40 % in the overall effectiveness is observed at $X/D_f = 20$ for the forward injection and 28% for the reverse injection because of the gas radiation which corresponds to a temperature rise of 194 K and 134 K respectively for forward and reverse injection at the metallic plate.

Declaration of Competing Interest

The authors declare that they have no known competing financial interests or personal relationships that could have appeared to influence the work reported in this paper.

References

[1] J. Issac, D. Singh, S. Kango, Experimental and numerical investigation of heat transfer characteristics of jet impingement on a flat plate, Heat Mass Transf. 56 (2) (2020) 531–546.

[2] S. Dutta, P. Singh, Opportunities in jet-impingement cooling for gas-turbine engines, Energies 14 (6587) (2021) 1–29.

[3] J. Zhang, S. Zhang, C. Wang, X. Tan, Recent advances in film cooling enhancement: A review, Chin. J. Aeronaut. 33 (4) (2020) 1119–1136.

[4] D.H. Lee, S.H. Oh, E.Y. Jung, K.M. Kim, H.H. Cho, Effect of array jet on cooling effectiveness on full-coverage film cooled surface, in: Proceedings of ASME 2009 Heat Transfer Summer Conference, San Francisco, California USA, July 19–23, 2009.

[5] R.K. Panda, B.V.S.S.S. Prasad, Conjugate heat transfer from a flat plate with combined impingement and film cooling, in: Proceedings of ASME Turbo Expo 2012, Copenhagen, Denmark, June 11–15, 2012.

[6] A. Mensch, K.A. Thole, Overall effectiveness of a blade endwall with jet impingement and film cooling, J. Eng. Gas Turbines Power 136 (2014) 031901.

[7] E.Y. Jung, H. Chung, S.M. Choi, T. Woo, H.H. Cho, Conjugate heat transfer on full-coverage film cooling with array impingement jets, in: Proceedings of ASME Turbo Expo 2015: Turbine Technical Conference and Exposition GT2015, Montreal, Canada, June 15–19, 2015.

[8] E.Y. Jung, H. Chung, S.M. Choi, T.-K. Woo, H.H. Cho, Conjugate heat transfer on full-coverage film cooling with array jet impingements with various Biot numbers, Exp. Therm Fluid Sci. 83 (2017) 1–8.

[9] Z. Liu, L. Ye, Z. Feng, Numerical study of impingement and film composite cooling on blade leading edge, in: Proceedings of ASME Turbo Expo 2014: Turbine Technical Conference and Exposition GT2014, Düsseldorf, Germany, June 16–20, 2014.

[10] A. Mensch, K.A. Thole, B.A. Craven, Conjugate heat transfer measurements and predictions of a blade endwall with a thermal barrier coating, J. Turbomach. 136 (2014) 121003.

[11] A. Mensch, K.A. Thole, Conjugate heat transfer analysis of the effects of impingement channel height for a turbine blade endwall, Int. J. Heat Mass Transf. 82 (2015) 66–77.

[12] X.C. Li, P. Corder, Characteristics of cooling of the leading edge with a row of dual impinging jets, in: Proceedings of 2008 ASME Summer Heat Transfer Conference, Jacksonville, Florida USA, August 10–14, 2008.

[13] S. Ravelli, L. Dobrowolski, D.G. Bogard, Evaluating the effects of internal impingement cooling on a film cooled turbine blade leading edge, in: Proceedings

[14] Y. Wei-hua, C. Jun, S. Rui, H. Xu-sheng, S. Shuang-wen, Experimental investigation on impingement-effusion film-cooling behaviors in curve section, Acta Astronaut. 68 (11–12) (2011) 1782–1789.

[15] Z. Liu, L.v. Ye, C. Wang, Z. Feng, Numerical simulation on impingement and film composite cooling of blade leading edge model for gas turbine, Appl. Therm. Eng. 73 (2) (2014) 1432–1443.

[16] D. Chandran, B. Prasad, Conjugate heat transfer study of combined impingement and showerhead film cooling near NGV leading edge, Int. J. Rotat. Mach. 2015 (2015) 1–13.

[17] X. Yang, Z. Liu, Q. Zhao, Z. Liu, Z. Feng, F. Guo, L. Ding, T.W. Simon, Experimental and numerical investigations of overall cooling effectiveness on a vane endwall with jet impingement and film cooling, Appl. Therm. Eng. 148 (2019) 1148–1163.

[18] J.-M. Miao, C.-Y. Wu, Numerical approach to hole shape effect on film cooling effectiveness over flat plate including internal impingement cooling chamber, Int. J. Heat Mass Transf. 49 (5–6) (2006) 919–938.

[19] S.H. Oh, D.H. Lee, K.M. Kim, M.Y. Kim, H.H. Cho, Enhanced cooling effectiveness in full-coverage film cooling system with impingement jets, in: Proceedings of ASME Turbo Expo 2008: Power for Land, Sea and Air, Berlin, Germany, June 9–13, 2008.

[20] J. Mao, Z. Liu, W. Guo, J. Zeng, Experimental studies on cooling effectiveness of the double-decker air jet impingement with film outflow, in: Proceedings of GT2007, ASME Turbo Expo 2007: Power for Land, Sea and Air, Montreal, Canada, May 14–17, 2007.

[21] E.Y. Jung, D.H. Lee, S.H. Oh, K.M. Kim, H.H. Cho, Total cooling effectiveness on a staggered full-coverage film cooling plate with impinging jet, in: Proceedings of ASME Turbo Expo 2010: Power for Land, Sea and Air, Glasgow, UK, June 14–18, 2010.

[22] R.K. Panda, B.V.S.S.S. Prasad, Conjugate heat transfer from an impingement and film-cooled flat plate, J. Thermophys. Heat Transf. 28 (4) (2014) 647–666.

[23] X. Yang, Z. Liu, Z. Liu, B. Wu, Z. Feng, Influence of jet impingement configurations and aerothermal variables on film cooling, in: Proceedings of ASME Turbo Expo 2016: Turbomachinery Technical Conference and Exposition GT2016, Seoul, South Korea, June 13–17, 2016.

[24] A.K. Singh, K. Singh, D. Singh, N. Sahoo, Large eddy simulations for film cooling assessment of cylindrical and laidback fan-shaped holes with reverse injection, J. Therm. Sci. Eng. Appl. 13 (2021) 1–16, https://doi.org/10.1115/1.4048679.

[25] K. Singh, B. Premachandran, M.R. Ravi, Experimental and numerical studies on film cooling with reverse/backward coolant injection, Int. J. Therm. Sci. 111 (2017) 390–408, https://doi.org/10.1016/j.ijthermalsci.2016.09.027.

[26] F. Tong, W. Gou, W. Gao, L. Li, Z. Yue, Numerical investigation of impinging-film heat transfer and flow characteristics of turbine inner casing, in: Proceedings of the ASME 2018 5th Joint US-European Fluids Engineering Division Summer Meeting FEDSM2018, Montreal, Quebec, Canada, July 15–20, 2018.

[27] K. Singh, B. Premachandran, M.R. Ravi, Effect of thermal barrier coating and gas radiation on film cooling of a corrugated surface, J. Heat Transfer 140 (2018) 094504.

[28] Ansys Fluent 14.5. User's and theory guide. Canonsburg, Pennsylvania, USA: ANSYS, Inc., 2014.

[29] Udayraj, P. Talukdar, A. Das, R. Alagirusamy, Alagirusamy, Design and development of a test method for analyzing protective performance of gloves exposed to radiant heat based on computational fluid dynamics analysis, Heat Transf. Eng. 40 (1–2) (2019) 95–108, https://doi.org/10.1080/01457632.2017.1404833.

[30] S.R. Turns, Thermal Fluid Science-An Integral Approach, Cambridge University Press, New York, NY, 2006.

[31] A. Kermanpur, N. Varahram, P. Davami, M. Rappaz, Thermal and grain-structure simulation in a land-based turbine blade directionally solidifed with the liquid

metal cooling process, Metall. Mater. Trans. B 31B (2000) 1293–1304.

[32] R. Vassen, X. Cao, F. Tietz, D. Basu, D. Stöver, Zirconates as new materials for thermal barrier coatings, J. Am. Ceram. Soc. 83 (8) (2000) 2023–2028.

[33] K.W. Schlichting, N.P. Padture, P.G. Klemens, Thermal conductivity of dense and porous yttria-stabilized zirconia, J. Mater. Sci. 36 (12) (2001) 3003–3010.

[34] H.I.H. Saravanamuttoo, G.F.C. Rogers, H. Cohen, P.V. Straznicky, Gas Turbine Theory, sixth ed., Pearson Education Limited, 2009.

[35] S. Baheri, B.A. Jubran, S.P.A. Tabrizi, The effect of turbulence intensity on film cooling of gas turbine blade from trenched shaped holes, in: Proceedings of ASME Turbo Expo 2008: Power for Land, Sea and Air, Berlin, Germany, June 09–13, 2008.

[36] W. Wenping, S. Peng, R. Jing, J. Hongde, Radiative effectiveness on the aero- and thermodynamics in a highly thermally loaded film cooling system. Proceedings of ASME Turbo Expo 2011 GT2011, 2011.

[37] S.V. Patankar, Numerical Heat Transfer and Fluid Flow, Hemisphere, Washington, DC, 1990.

[38] M. Silieti, A.J. Kassab, E. Divo, Film cooling effectiveness: comparison of adiabatic and conjugate heat transfer CFD models, Int. J. Therm. Sci. 48 (12) (2009) 2237–2248.

[39] I.B. Celik, J. Li, Assessment of numerical uncertainty for the calculations of turbulent flow over a backward-facing step, Int. J. Numer. Meth. Fluids 49 (9) (2005) 1015–1031, https://doi.org/10.1002/fld.1040.

[40] S. Eshati, A. Abu, P. Laskaridis, A. Haslam, Investigation into the effects of operating conditions and design parameters on the creep life of high pressure turbine blades in a stationary gas turbine engine, Mech. Mech. Eng. 15 (3) (2011) 237–247.

[41] M. Rezazadeh Reyhani, M. Alizadeh, A. Fathi, H. Khaledi, Turbine blade temperature calculation and life estimation - a sensitivity analysis, Propuls. Power Res. 2 (2) (2013) 148–161.

[42] K. Singh, B. Premachandran, M.R. Ravi, Experimental and numerical studies on film cooling of a corrugated surface, Appl. Therm. Eng. 108 (2016) 312–329.

[43] Y. Levy, A.G. Rao, V. Erenburg, V. Sherbaum, I. Gaissinski, V. Krapp, Pressure losses for jet array impingement with crossflow, in: Proc. ASME Turbo Expo, GT2012-68386, 2012, pp. 139–149. https://doi.org/10.1115/GT2012-68386.

[44] P.S. Penumadu, A.G. Rao, Numerical investigations of heat transfer and pressure drop characteristics in multiple jet impingement system, Appl. Therm. Eng. 110 (2017) 1511–1524, https://doi.org/10.1016/j.applthermaleng.2016.09.057.

[45] J. Ren, X. Li, H. Jiang, Conjugate heat transfer characteristics in a highly thermally loaded film cooling configuration with TBC in syngas, Aerospace 6 (2) (2019) 16.